Wall Climbing Emergent Behavior in a Swarm of Real-World Miniature Autonomous Blimps

Tristan K. Schuler[1][a], Cameron Kabacinski[2], Daniel M. Lofaro[1], Dhawal Bhanderi[2],
Jennifer Nguyen[2] and Donald Sofge[1][b]

[1]*Navy Center for Applied Research in AI (NCARAI), U.S. Naval Research Laboratory, Washington D.C, 20375, U.S.A.*
[2]*Intern, U.S. Naval Research Laboratory, Washington D.C., 20375, U.S.A.*

Abstract: Emergent behaviors in swarms can arise when agents with simple behavioral rules produce complex group dynamics. In this work we develop both a physics-based simulation environment as well as a real-world testbed for indoor miniature autonomous blimps to analyze sensor-driven emergent behavior. During the flight experiments, the blimps had global localization from an indoor motion capture system to follow waypoints but used downward facing ultrasonic ping sensors for local-frame altitude control. After introducing a wall to the environment and commanding the swarm to the other side of the unknown obstacle, a wall climbing emergent behavior arose where the swarm agents climbed over each other as well as the wall to reach the goal. We demonstrate how modifying the sensor characteristics between trials and changing the swarm size affects this emergent behavior in both simulation and with real-world blimps, and compare the results.

1 INTRODUCTION

Emergent behavior can arise in swarms when an agent with simple behavioral rules can produce complex group dynamics. There are many instances of emergent behavior arising in nature, especially with social insects. One of the most popular emergent behavior models is for the flocking of birds or fish where the initial conditions can lead to a common velocity for the flock (Cucker and Smale, 2007). Foraging ants leave behind pheromones during foraging which other ants follow and continue to reinforce, creating a "highway" of ant traffic to the goal, typically food (Bonabeau et al., 1997). Under certain conditions, army ants will form "living bridges' where they will climb on top of one another to reach a goal faster (Graham et al., 2017). Similarly, fire ants self-assemble to build towers as temporary shelters, especially after flooding, a process that randomly emerges (Phonekeo et al., 2017). Honeybees self-organize for honeycomb creation and an overall pattern emerges spontaneously from dynamic interactions among the processes of depositing and removing brood, pollen and honey (Camazine, 1991).

[a] https://orcid.org/0000-0002-1567-322X
[b] https://orcid.org/0000-0003-0153-3581

A common limitation to simulating swarm behavior and algorithms is that there are frequently many assumptions made such as only focusing on dynamic behavior, having perfect communication, no catastrophic collisions, or even having agents with negligible size (Taylor and Nowzari, 2021). Several swarm robot platforms and algorithm development efforts have been inspired by nature. Researchers at Harvard developed the Bluebot underwater fish platform and demonstrated common emergent behavior algorithms on real agents, such as the ring state, and could also sustain collisions with the tank and other agents (Berlinger et al., 2021). Researchers at the University of Alabama explored waypoint navigation with collidable micro-airships (Troub et al., 2017). The GRASP lab at University of Pennsylvania developed small UAVs that are capable of sustaining collisions and then able to navigate without complete knowledge of the environment, and then create a sparse map of their surroundings (Mulgaonkar et al., 2017; Mulgaonkar et al., 2020). Another group used simple robots with binary tactile sensors to determine if a collision occurred and let the agents use this information for probabilistic localization (Mayya et al., 2017; Mayya et al., 2018). Similarly, researchers at ETH Zurich demonstrated navigation through an unknown environment and low-level mapping by ex-

225

ploiting collision information from an onboard IMU (Lew et al., 2019). In this work, we try to bridge the gap between simulated and real-world swarms using an indoor autonomous blimp robotic platform.

Indoor lighter-than-air vehicles are a great robotic platform for testing emergent behaviors on real-world robots. One of the major benefits to lighter-than-air vehicles is that they can move in a 3D environment with other agents without needing to account for the possibility of catastrophic collisions. In this paper we use the *Georgia Tech Miniature Autonomous Blimps* (GT-MAB) platform for producing wall-climbing emergent behavior on real-world agents in a 3D space (Cho et al., 2017). In 2019, researchers at the U.S. Naval Research Laboratory demonstrated formation flying with 25+ modified versions of the GT-MAB, the largest real-world demonstration of indoor autonomous blimps to date (Schuler et al., 2019). Additional recent research with this platform includes time synchronized path planning, indoor localization, human interaction, and gesture control (Gibson et al., 2020; Yao et al., 2019; Yao et al., 2017; Seguin et al., 2020; Srivastava et al., 2019). Researchers at the U.S. Naval Research Laboratory also explored swarm behavior in lighter-than-air vehicles using universal global inputs from onboard sensing as well as exploring visoelastic fluid-inspired swarm behavior (Hall et al., 2021; McGuire et al., 2021).

In this paper, we set up an emergent behavior test bed for miniature autonomous blimps in both simulation and the real-world where the blimps climb an unknown wall due to the inclusion of a downward ultrasonic ping sensor for altitude control. We also explore how adjusting the sensor characteristics or parameters affects the emergent behavior. Additionally, this paper discusses the development of a physics based physics-based simulator capable of testing large swarm sizes of indoor blimps. The simulator is validated by comparing the performance to real world experiments with a smaller swarm of real-world agents.

2 WALL CLIMBING TESTBED

In our 2019 experiment using 25+ GT-MABs for formation control, the agents used Vicon, an indoor infrared motion capture system, for horizontal waypoint navigation. We installed downward-facing ultrasonic ping sensors on the blimp gondola to do local-frame altitude control. In the flight demonstration we also manually drove a Pioneer ground rover, shown In Figure 1, underneath the autonomous blimp formation and demonstrated that individual agents rose after detecting a local-frame altitude change from the Pioneer
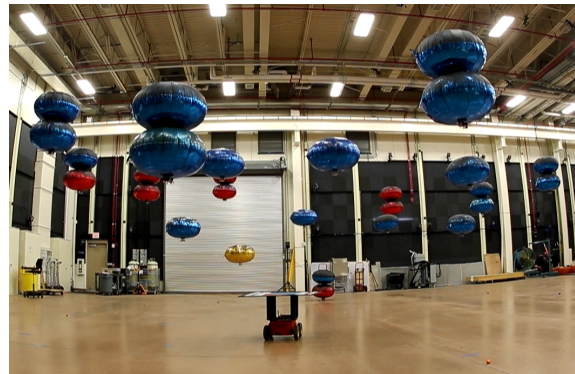

Figure 1: 25+ blimp swarm experiment where wall climbing phenomenon was discovered.

underneath. Occasionally, a blimp would drift away from its target waypoint due to either HVAC currents, hardware malfunctions, or occluded motion capture markers. Some of these drifting agents would reach a wall and start "climbing" it. The climbing phenomenon arose from the downward facing ultrasonic ping sensor detecting the wall and triggering an upward velocity to reach the target altitude, which was never obtained since the wall was in range. This introduced the question of whether or not a group of blimps with simple sensing could overcome obstacles without path-planning. We hypothesized that a swarm of blimps could climb a wall without knowledge of the obstacle, and that the success rate of reaching the other side of the wall could change by adjusting sensor characteristics and the swarm size.

2.1 Agent Design

The lighter-than-air agents used in these experiments are a modified version of the GT-MAB agents. The GT-MABs are helium filled lighter-than-air vehicles with a customized gondola attached to standard 36" Mylar balloon envelopes. The gondola contains five motor/propeller pairs for holonomic motion: two for altitude control, two for forwards/backwards and yaw control, and one for lateral control. Additionally, the gondola also contains the motor controller, battery, and XBee radio for communicating with a host computer. For indoor localization, the agents were equipped with retro-reflective Vicon markers on the tops of the envelopes. We lightly spray painted the tops of the envelopes to reduce noisy reflections from the metallic Mylar envelope.

The modified GT-MABs incorporate a downward facing ultrasonic ping sensor for altitude control or obstacle avoidance and can be seen in Figure 2. The ultrasonic ping sensor implementation was designed to be modular, so that different ping sensors, with
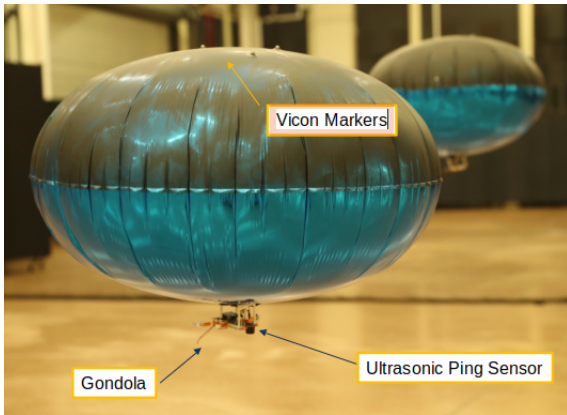
Figure 2: Modified *Georgia Tech Miniature Autonomous Blimps* (GT-MAB) with downward facing ultrasonic sensors for altitude control, and Vicon markers for localization.
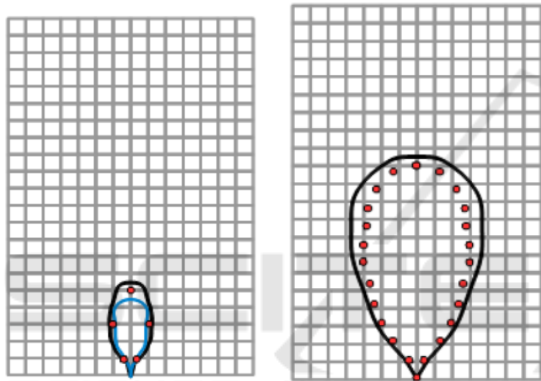

Figure 3: MaxSonar Ultrasonic Ping Sensor beam width estimates for 30cm grid resolution and tested with a 3.5 inch diameter dowel. Image 1 is narrowest beam width, and image 2 is widest beam width available.

varying beam widths could easily be installed on each. For these experiments we used two variations of MaxSonar Ultrasonic ping sensors, the narrowest and widest variations. Figure 3 shows the difference between the narrow-beam and wide-beam sensors. Both sensors have a maximum altitude range of 5.0 m but significantly different proximity cones for detecting ultrasonic pings. For these experiments we use the same controller architecture as our 25+ lighter-than-air autonomous agents demonstration; horizontal motion was controlled from motion-capture feedback and altitude was controlled from ultrasonic ping feedback (Schuler et al., 2019).

2.2 Control Structure

Both the real-world and simulated blimps used a control architecture of 4 independent proportional-derivative (PD) feedback controllers for horizontal

position, yaw orientation, and altitude. The controller PD outputs denoted as $u_{x_{global}}$, $u_{y_{global}}$, $u_{z_{local}}$ are calculated separately by:

$$u_j = K_{pj}e_{pj} + K_{ij}\int_0^t e_{pj}dt' + K_{dj}\frac{de_{pj}}{dt} \qquad (1)$$

where $j = \{x_{global}, y_{global}, z_{local}\}$, e_{pj} is the Euclidean error, and K_p, K_i, and K_d are the proportional, integral and derivative gains.

A fourth PD controller for yaw about the global z-axis is defined by:

$$u_\theta = K_p^\theta e_\theta + K_i^\theta \int_0^t e_\theta dt + K_d^\theta \frac{de_\theta}{dt} \qquad (2)$$

where u_θ is the resulting control rotational velocity about the z-axis and e_θ is the error between the desired orientation about z and the measured orientation. K_p^θ, K_i^θ, and K_d^θ are the proportional, integral and derivative gains for the yaw controller.

The output of these 4 independent PD controllers were velocities $\dot{x}$, $\dot{y}$, $\dot{z}$, and $\dot{\theta}_z$:

$$[\dot{x}, \dot{y}, \dot{z}, \dot{\theta}_z] \qquad (3)$$

2.3 Simulation Environment

We developed a physics-based simulation environment to run experiments that would be challenging to implement with real-world agents such as larger swarm sizes and additional sensor characteristic differences.

2.3.1 Simulation Architecture

The simulation architecture was developed in CoppeliaSim, previously known as VREP (Rohmer et al., 2013). CoppeliaSim enables building dynamic robot models out of simple and complex shapes that respond to the environment, and allows individual agent control through their own script. The simulator is controlled through API calls to start/stop the simulation and manipulate objects, which allows for simulation automation and data collection.

2.3.2 Matching Simulated Blimps to GT-MAB

The simulated agents were matched to the physical attributes of the real-world modified GT-MAB. Each component, including the motors, envelope, gondola, battery, and ballast, was measured and weighed, and then recreated in simulation using simple shapes to create a 1:1 scale model of the agent.

To make the simulation as realistic as possible, real-world blimp characteristics were measured and

applied to the simulated agents. The most relevant characteristics included measuring the maximum force of a single motor, the blimp's buoyancy, the maximum velocity of the blimp, and approximate angular dampening. Coppeliasim does not directly support lift or aerodynamic simulation, so additional forces are necessary to be applied to the model at each simulation time step. Each agent's control script directly interfaces with the simulated motors by applying a force at the motor locations and limited by the measured maximum motor force.

To offset gravity and provide buoyancy, a constant upward force is applied to the model's center of mass to estimate the lift force provided by the helium-filled envelope. The exact force is based on the simulated weight and a small ballast adjustment to provide proper buoyancy (slightly below neutral). The buoyancy characteristic was determined by dropping the real blimp from a set height and recording the time it took to fall, and then calibrating the ballast adjustment in simulation.

To ensure a correct maximum achievable velocity, a drag force was calculated and applied to the center of mass at every simulation step. The drag force is presented in Eq. 4 where F_d is the drag force, ρ is the air density, v is the velocity, c_d is the drag coefficient, and A is the cross-section area. While each variable in the drag force equation could be found independently, by grouping ρ, A, c_d, and the 1/2 factor together as β, the drag force equation becomes simplified, as shown in Eq. 5.

The blimp's real world characteristics can be leveraged to find β as there are only two unknowns, F_d and v, both of which can be found when the blimp is moving with full forward throttle. The blimp's maximum velocity happens when the blimp is no longer able to accelerate and reaches a force balance, which occurs when the two forward facing motors provide a force equal to the drag force, as shown in Eq. 6, where F_m is the maximum force of a single motor. The maximum velocity is measured by tracking the blimp position over time. Thus, β will equal the maximum force provided by the forward motors divided by the maximum velocity squared, shown in Eq. 7.

$$F_d = \frac{1}{2}\rho v^2 c_d A \qquad (4)$$

$$\beta = \frac{1}{2}\rho c_d A, \quad F_d = \beta v^2 \qquad (5)$$

$$F_{net} = ma, \quad 2F_m - F_d = 0, \quad F_d = 2F_m \qquad (6)$$
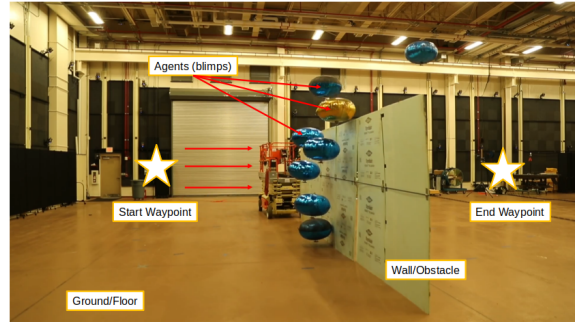
$$\frac{2F_m}{v_{MAX}^2} = \beta \qquad (7)$$

Figure 4: Real-world wall climbing testbed with 8 autonomous blimps equipped with downward facing ultrasonic sensors for altitude control.

Once β was found, at each simulation step, the blimp velocity could be calculated by the simulator and multiplied by β to find the drag force, as in Eq. 5, and applied to the center of the blimp.

Additionally angular dampening was added to the simulated agents to match real-world agents. Without any angular dampening, applied motor forces in simulation caused a torque around the center of mass which creates a rocking pendulum motion that is not observed in the real world. The real blimp was held at a 45-degree angle relative to the horizon and released and timed until it settled back to horizontal equilibrium. Then, the simulated blimp was setup the same and angular dampening coefficients were tuned until the settle time was the same between the real and simulated models.

Finally, a proximity sensor was added with matching characteristics to the ultrasonic ping sensor installed on the real-world gondolas shown in Figure 3. A Gaussian noise distribution was added to the sensor feedback to simulate noise from the real sensor as well as inconsistencies with altitude holding due to additional unknown forces such as unknown air flows or propeller wash. The same PD controller structure from Section 2.2 was implemented on the simulated agents for waypoint navigation with local altitude sensing from the proximity sensor.

2.4 Experimental Setup

The simulation environment was setup with the same parameters as the real-world experiment. A 2.5 m wall was placed perpendicular to the desired path of motion between the start and end way points. All agents in the swarm were given the same starting and ending waypoint in each trial. The agents had global localization knowledge in the X-Y plane but used a downward facing ultrasonic ping sensor for local-frame altitude control. The agents then had 5 minutes to attempt to maneuver to the other side of the un-
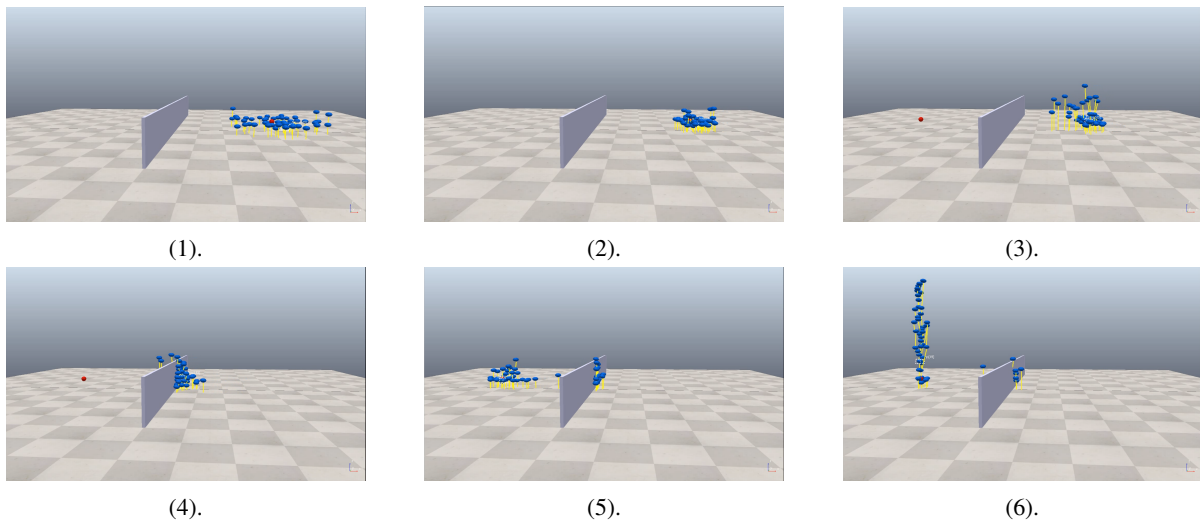
(1).

(2).

(3).

(4).

(5).

(6).

Figure 5: Fifty simulated autonomous blimps with a local altitude setpoint of 1.0 m and 20 s to reach starting waypoint after initial random distribution (1-2). After 20 s the group waypoint is set to the opposite of the side of the wall; the swarm attempts to move to the waypoint (3-5). The blimps start "towering" with extended time at a target waypoint (6).

known wall. Figure 4 shows the real-world set up of the experiment.

Figure 5 shows snapshots of a simulated wall climbing trial with 50 agents at a 1.0 m local-frame altitude setpoint. At the start of a trial, the agents were randomly distributed on one side of the wall and had a 20 s period to maneuver to the starting X-Y waypoint coordinate centered on the same side of the wall as the swarm, shown in the first two images of Figure 5. After 20 s, the waypoint changed to an X-Y coordinate centered on the other side of the wall, and the agents immediately try to maneuver to the new waypoint. The agents were unaware of the wall and their global altitude, only their global X-Y position and local altitude readings from the downward facing proximity sensors. An emergent behavior arose where the blimps "climbed" the wall as well as other nearby agents while trying to maneuver to the new waypoint, shown in images 3-6 in Figure 5. By changing sensor characteristics such as the altitude set point and beam width, as well as the swarm size, the success rate of the wall climbing emergent behavior changed.

Additionally, a secondary emergent behavior of "towering" occasionally occurred at the starting or ending waypoints when the swarm has extended time at the waypoint. Figure 6 shows the towering behavior in simulated and real world agents. Towering occurs when an agent floats above another and triggers a new local-frame altitude reading from the ultrasonic sensor. The balloons do not start in a towering formation, but can maneuver on top of other agents for several reasons including collisions from other agents, prop wash from other agents, and sensor noise causing oscillating altitude control. Towering can happen
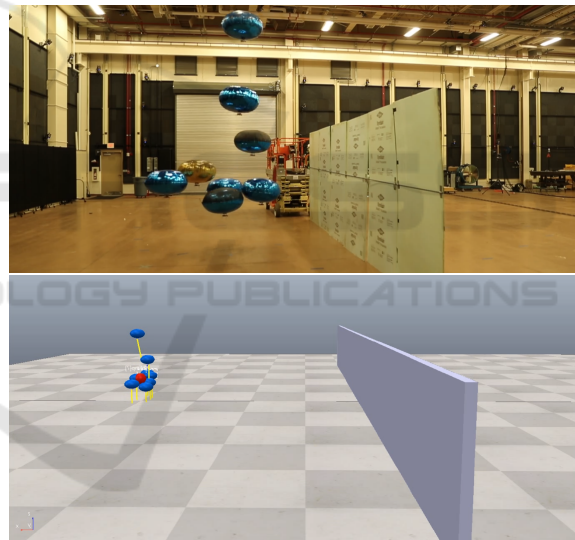

Figure 6: Towering emergent behavior with an 8 agent swarm in both real-world and simulated blimps.

with as little as two agents, but is more prominent with larger swarms.

Multiple trials were simulated and conducted with physical agents with varying sensor characteristics including beam width and altitude set point, as well as varying the size of the swarm to observe effects on the wall-climbing emergent behavior. Wall climbing success was binary for individual agents; an individual success was denoted by crossing the plane of the wall. The overall success rate of the swarm was then the average percentage of agents that made it to the other side of the wall. Five (5) trials were conducted for each set of independent variables with the swarm
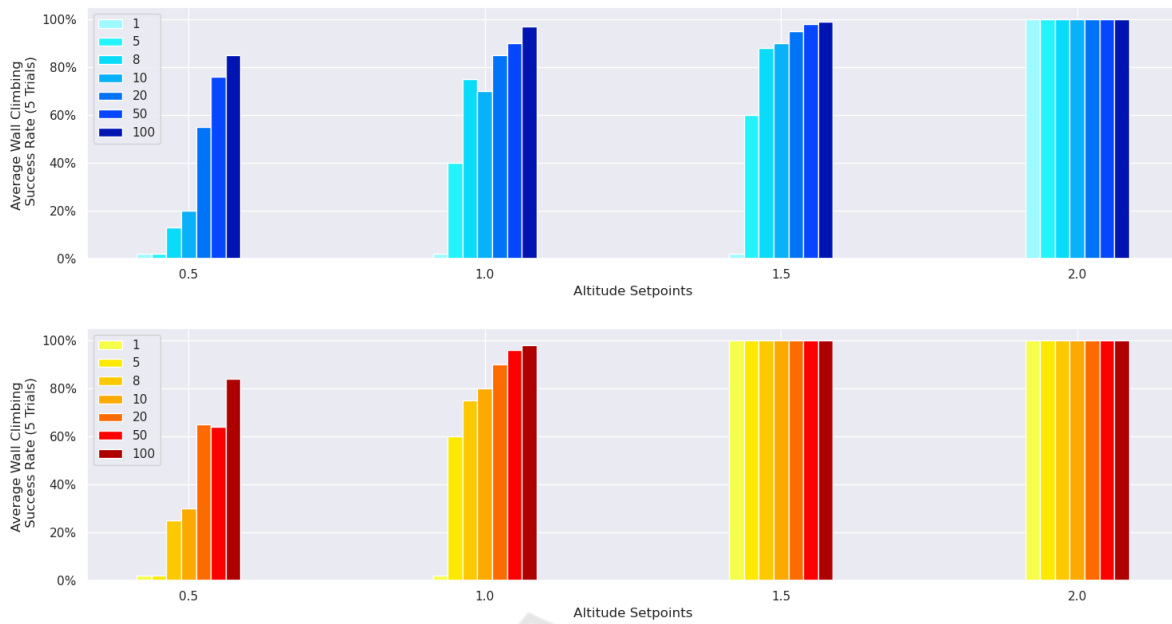
Figure 7: Simulated wall climbing success rates for downward facing narrow-beam-width proximity sensor (top) and wide-beam-width (bottom) sensor for varying altitude setpoints and swarm sizes (color gradients).

wall climbing success rates averaged. The independent variables in each trial included local-frame altitude setpoint from proximity sensor (0.5m, 1.0m, 1.5m, and 2.0m), proximity sensor beamwidth (narrow, wide), and swarm size (1, 5, 8, 10, 20, 50, and 100 agents).

3 RESULTS & DISCUSSION

Figure 7 shows the simulated swarm's average wall climbing success rates (along y-axis) after 5 trials for 3 varying parameters: proximity sensor beam width (narrow on top, wide on bottom), swarm size (colored gradient), and the altitude set point (along x-axis). As hypothesized, both a larger swarm size and higher altitude set points increased the overall swarm wall-climbing success rate. The 2.0 m altitude setpoint resulted in a 100% wall climbing success rate for any number of simulated agents for both the wide and narrow proximity sensor. Surprisingly, the wide-angle proximity sensor had minimal effect on the wall climbing success rate, both on simulated agents and the real-world agents. On average, the wide-angle ultrasonic sensor produced a 5-10% increase in wall climbing success rate compared with the narrow beam width sensor. This gap in performance between the narrow and wide beam width sensors also decreased the larger the swarm size was. Therefore, like the real-world experiments, the altitude set point was the driv-
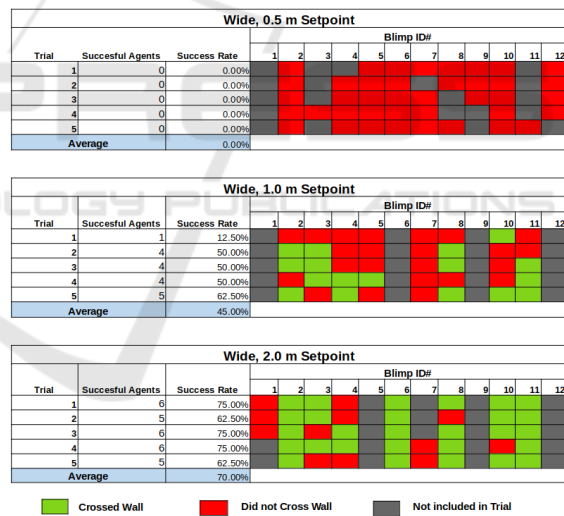

Figure 8: Wall climbing success rate for real-world blimps equipped with wide angle ultrasonic ping sensors at various altitude setpoints.

ing force for wall climbing emergent behavior, not the beamwidth of the sensor.

Similar trials were conducted with a swarm of 8 real-world blimps. Figure 8 shows the individual trials of the 8-agent swarm. For the most part, the agents that successfully crossed the wall were random between trials; however, there were exceptions. Throughout the trials, blimp #7 never crossed the wall although it was fully operational. Similarly, in the 2.0
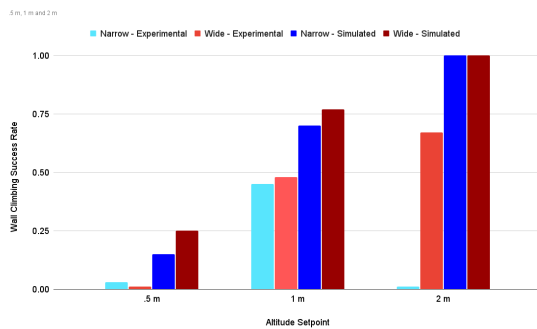
Figure 9: Experimental and simulated wall climbing success rate for 8 real-world blimps at various altitude setpoints and ping sensor beam widths.

m experiments blimps #2, #6, and #11 made it across the wall every time.

Figure 9 shows the wall climbing success rate difference between simulation and the real-world experiment for an 8-agent swarm. The overall trend was similar, with a higher altitude setpoint resulting in a higher wall climbing success rate for both simulated and real-world agents. However, the simulated environment had higher success rates for each altitude setpoint. The 2.0 m setpoint had a 100% success rate for simulated agents whereas only 65% of the swarm made it across on average with the real-world blimps.

It is important to note that the simulated agents perform better than the real-world agents, for many reasons. While efforts were made to match the simulation to the dynamics of the real-world blimps, as discussed in section 2.3.2 there's still many unknown or hard to simulate variables. A major inconsistency that's challenging to simulate is random hardware malfunctions or failures, which happened frequently. The most common hardware issues were typically motors with weakened thrust profiles after frequent use or communication issues with either the mission control computer, or the motion capture system. These hardware issues were a major reason why we felt the need to develop a MAB simulator to test larger swarms of MABs without constantly making robot repairs or solving the hard problem of indoor global localization with a large number of agents.

The gray numbered blimps in Figure 8 shows blimps that were not included in the trials. These were typically hardware issues that could be repaired or fixed in between trials, but sometimes the issue was a permanent failure that required hardware replacement. The required ballast and buoyancy force varies from blimp to blimp due to helium leakage and requires occasional refilling before experiments. Additionally, small changes in temperature as well as internal drafts from the HVAC system or other miscella-

neous indoor currents can also have major effects on blimp performance; while these two variables could be simulated, they are hard to accurately match to the real-world testbed.

4 CONCLUSIONS AND FUTURE WORK

In this work we develop a simulation and experimental environment for exploring emergent behaviors in swarms of indoor miniature autonomous blimps. We demonstrate a wall climbing emergent behavior in a swarm of autonomous blimps experimentally and in simulation through changing the characteristics of a very simple ultrasonic ping sensor and the swarm size. As the local-frame altitude set point increases, the success rate of wall climbing increases; also, as the swarm size increases, the wall climbing success rate increases. With extended time at a group waypoint, a secondary emergent behavior of "towering" would also occasionally occur.

In the future we would like to change the control scheme to explicitly include potential fields to see if the emergent behavior changes, as well as add more known and unknown obstacles. In these experiments the individual agents' behavior mimics 2D potential fields in an unknown environment. There is an attractive force in the XY plane attracting all of the agents to the other side of the room and a repulsive force along the Z-axis from the floor, wall, and other agents all acting as repulsive forces. Typically, the wall acts as a local maximum for individual agents with a low altitude setpoint (<1.5). However, with a large enough swarm, the attractive force can overcome the cumulative repulsive forces from other agents when they all reach the wall. We would also like to test the emergent behaviors with different styles of indoor autonomous blimp platforms that are currently used in the research community such as flapping wing blimps, cigar-shaped and fish-inspired blimps, and spherical blimps (Lin et al., 2022). Different shapes and sizes of blimps will introduce varying motion profiles, agility, controllability, and additional sensing capability on larger blimps.

REFERENCES

Berlinger, F., Gauci, M., and Nagpal, R. (2021). Implicit coordination for 3d underwater collective behaviors in a fish-inspired robot swarm. *Science Robotics*, 6(50).

Bonabeau, E., Theraulaz, G., Deneubourg, J.-L., Aron, S., and Camazine, S. (1997). Self-organization in social insects. *Trends in ecology & evolution*, 12(5):188–193.

Camazine, S. (1991). Self-organizing pattern formation on the combs of honey bee colonies. *Behavioral ecology and sociobiology*, 28(1):61–76.

Cho, S., Mishra, V., Tao, Q., Vamell, P., King-Smith, M., Muni, A., Smallwood, W., and Zhang, F. (2017). Autopilot design for a class of miniature autonomous blimps. In *2017 IEEE conference on control technology and applications (CCTA)*, pages 841–846. IEEE.

Cucker, F. and Smale, S. (2007). Emergent behavior in flocks. *IEEE Transactions on automatic control*, 52(5):852–862.

Gibson, J., Schuler, T., McGuire, L., Lofaro, D. M., and Sofge, D. (2020). Swarm and multi-agent time-based a* path planning for lighter-than-air systems. *Unmanned Systems*, 8(03):253–260.

Graham, J. M., Kao, A. B., Wilhelm, D. A., and Garnier, S. (2017). Optimal construction of army ant living bridges. *Journal of theoretical biology*, 435:184–198.

Hall, R., Maxseiner, A., Matejevich, B., Sofge, D. A., and Lofaro, D. M. (2021). Emergent behavior in swarms with on-board sensing. In *2021 IEEE Symposium Series on Computational Intelligence (SSCI)*. IEEE.

Lew, T., Emmei, T., Fan, D. D., Bartlett, T., Santamaria-Navarro, A., Thakker, R., and Agha-mohammadi, A.-a. (2019). Contact inertial odometry: collisions are your friends. In *The International Symposium of Robotics Research*, pages 938–958. Springer.

Lin, T. X., Rossouw, M., Maxseiner, A. B., Schuler, T., Garratt, M. A., Ravi, S., Zhang, F., Lofaro, D. M., and Sofge, D. A. (2022). Miniature autonomous blimps for indoor applications. In *AIAA SCITECH 2022 Forum*, page 1834.

Mayya, S., Pierpaoli, P., Nair, G., and Egerstedt, M. (2018). Localization in densely packed swarms using inter-robot collisions as a sensing modality. *IEEE Transactions on Robotics*, 35(1):21–34.

Mayya, S., Pierpaoli, P., Nair, G. N., and Egerstedt, M. (2017). Collisions as information sources in densely packed multi-robot systems under mean-field approximations. In *Robotics: Science and Systems*, volume 13.

McGuire, L., Schuler, T., Otte, M., and Sofge, D. (2021). Viscoelastic fluid-inspired swarm behavior to reduce susceptibility to local minima: The chain siphon algorithm. *IEEE Robotics and Automation Letters*, 7(2):1000–1007.

Mulgaonkar, Y., Liu, W., Thakur, D., Daniilidis, K., Taylor, C. J., and Kumar, V. (2020). The tiercel: A novel autonomous micro aerial vehicle that can map the environment by flying into obstacles. In *2020 IEEE International Conference on Robotics and Automation (ICRA)*, pages 7448–7454. IEEE.

Mulgaonkar, Y., Makineni, A., Guerrero-Bonilla, L., and Kumar, V. (2017). Robust aerial robot swarms without collision avoidance. *IEEE Robotics and Automation Letters*, 3(1):596–603.

Phonekeo, S., Mlot, N., Monaenkova, D., Hu, D. L., and Tovey, C. (2017). Fire ants perpetually rebuild sinking towers. *Royal Society open science*, 4(7):170475.

Rohmer, E., Singh, S. P., and Freese, M. (2013). V-rep: A versatile and scalable robot simulation framework. In *2013 IEEE/RSJ International Conference on Intelligent Robots and Systems*, pages 1321–1326. IEEE.

Schuler, T., Lofaro, D., McGuire, L., Schroer, A., Lin, T., and Sofge, D. (2019). A study of robotic swarms and emergent behaviors using 25+ real-world lighter-than-air autonomous agents (lta3). In *2019 3rd International Symposium on Swarm Behavior and Bio-Inspired Robotics (SWARM)*.

Seguin, L., Zheng, J., Li, A., Tao, Q., and Zhang, F. (2020). A deep learning approach to localization for navigation on a miniature autonomous blimp. In *2020 IEEE 16th International Conference on Control & Automation (ICCA)*, pages 1130–1136. IEEE.

Srivastava, D., Lofaro, D., Schuler, T., and Sofge, D. (2019). Gesture-based interface for multi-agent and swarm formation control. In *2019 3rd International Symposium on Swarm Behavior and Bio-Inspired Robotics (SWARM)*.

Taylor, C. and Nowzari, C. (2021). The impact of catastrophic collisions and collision avoidance on a swarming behavior. *Robotics and Autonomous Systems*, 140:103754.

Troub, B., DePineuil, B., and Montalvo, C. (2017). Simulation analysis of a collision-tolerant micro-airship fleet. *Int'l Journal of Micro Air Vehicles*, 9(4):297–305.

Yao, N., Anaya, E., Tao, Q., Cho, S., Zheng, H., and Zhang, F. (2017). Monocular vision-based human following on miniature robotic blimp. In *2017 IEEE International Conference on Robotics and Automation (ICRA)*, pages 3244–3249. IEEE.

Yao, N.-s., Tao, Q.-y., Liu, W.-y., Liu, Z., Tian, Y., Wang, P.-y., Li, T., and Zhang, F. (2019). Autonomous flying blimp interaction with human in an indoor space. *Frontiers of Information Technology & Electronic Engineering*, 20(1):45–59.